Cryogenics 50 (2010) 582–590

Contents lists available at ScienceDirect

Cryogenics

journal homepage: www.elsevier.com/locate/cryogenics

# Improved performance of an engineering model cryogen free double adiabatic demagnetization refrigerator

J. Bartlett [a,*], G. Hardy [a], I.D. Hepburn [a], C. Brockley-Blatt [a], P. Coker [a], E. Crofts [a], B. Winter [a], S. Milward [b], R. Stafford-Allen [b], M. Brownhill [c], J. Reed [c], M. Linder [d], N. Rando [d]

[a] Mullard Space Science Laboratory, Dorking, Surrey RH5 6NT, England, United Kingdom
[b] Scientific Magnetics, Abingdon, Oxfordshire OX14 3DB, England, United Kingdom
[c] EADS Astrium Ltd., Stevenage, Hertfordshire SG1 2AS, England, United Kingdom
[d] ESTEC, ESA, 2200 AG Noordwijk, The Netherlands

ARTICLE INFO

*Article history:*
Received 24 June 2009
Received in revised form 2 February 2010
Accepted 22 February 2010

*Keywords:*
Adiabatic demagnetization (E)
Magnetoresistance (C)
Space cryogenics (F)
Cryogen free magnets (F)
Magnetic refrigeration (E)

ABSTRACT

This paper describes the design, development and performance of the engineering model double adiabatic demagnetization refrigerator (dADR) built and tested under contract to the European Space Agency for its former mission XEUS (now IXO). The dADR operates from a 4 K bath and has a measured recycle and hold time (with a parasitic load of 2.34 μW) at 50 mK of 15 h and 10 h, respectively. It is shown that the performance can be significantly improved by operating from a lower bath temperature and replacing the current heat switches with tungsten magnetoresistive (MR) heat switches, which significantly reduce the parasitic heat load. Performing the latter gives an anticipated recycle and hold time of 2 and 29 h (with a 1 μW applied heat load in addition to the parasitic load), respectively. Such improved performance allows for a reduction in mass of the dADR from 32 kg to 10 kg by operating from a 2.5 K bath (which could be reduced further by optimising the magnet design). Ultimately, continuous operation could be achieved by linking two dADRs to a common detector stage and operating them alternately. Based on this design the mass of the continuous ADR is estimated to be about 4.5 kg.



## 1. Introduction

A cryogen free space engineering model double adiabatic demagnetization refrigerator (dADR) has been built and tested under ESA contract in collaboration with EADS Astrium (Stevenage, UK). In this paper, we describe the system development as a continuation of the design and development presented in Hepburn et al. [1,2]. In addition, the current performance and the anticipated improved performance (by replacing the heat switches) are presented along with the design to extend the dADR to achieve continuous cooling.

The main driving requirements for the ADR were: (1) a cold finger temperature of 50 mK (with a target of 30 mK) for 24 h with a 1 μW heat load and with a 4 h ADR recycle time; (2) a maximum heat load to the ADR heat sink of <5 mW in order to allow cooling via a space cryocooler; (3) a magnetically shielded <5 μT (0.05 G) detector focal plane to house superconducting tunnel junction (STJ) or transition edge (TES) X-ray detector arrays and associated SQUID readout electronics; (4) magnetic screening of the whole system to reduce the exported stray magnetic flux density to a level acceptable to a spacecraft (<67 μT, <0.67 G). The ADR was developed based on the requirements for ESA's former proposed mission, the X-ray Evolving Universe Spectroscopy mission (XEUS) and as a generic technology. XEUS has now been merged with the former proposed NASA mission Constellation-X to form the International X-ray Observatory (IXO) which is a joint ESA–JAXA–NASA mission. IXO will have the same scientific goals as XEUS focussing on: (1) black holes and matter under extreme conditions; (2) formation and evolution of galaxies, clusters and large scale structures; (3) life cycles of matter and energy. The spacecraft, which will be placed in orbit at L2, will comprise of a single large X-ray mirror assembly, an extendible optical bench with a focal length of approximately 20 m and a suite of focal plane instruments including a cryogenic spectrometer, the X-ray Microcalorimeter Spectrometer (XMS). The XMS will use superconducting Transition Edge Sensors (TES) which are highly sensitive and require an operating temperature of 50 mK. This can be achieved by an adiabatic demagnetization refrigerator, pre-cooled by a space cryocooler which will enable the proposed lifetime of 5–10 years.

The engineering model (EM) dADR, was successfully delivered to ESA in July 2008 with the ADR remaining at MSSL as a test bed for continued testing and development. Upon delivery, the ADR fulfilled all requirements stated above with the exception of

* Corresponding author. Tel.: +44 1483 204206.
*E-mail address:* jb2@mssl.ucl.ac.uk (J. Bartlett).

0011-2275/$ - see front matter © 2010 Elsevier Ltd. All rights reserved.
doi:10.1016/j.cryogenics.2010.02.024

the recycle and hold times. By changing the heat switches, the ADR is expected to fulfil all of the design requirements. This is discussed in more detail in Section 4.

## 2. The engineering model ADR design

The ADR design is that of a double ADR (see Fig. 1) comprising of two different paramagnetic materials (pills) operating in series, with the high temperature pill (paramagnetic material 1 in Fig. 1) providing a low temperature heat sink for the low temperature pill (paramagnetic material 2). The high temperature stage is connected to both the heat bath and the low temperature stage via heat switches and both pills are suspended within the bore of their magnet via Kevlar cords (1.5 mm diameter for the high temperature stage and 0.75 mm diameter for the low temperature stage), providing relatively good thermal isolation when the heat switches are open. This design, in comparison to single and two-stage ADRs, enables the longest possible hold time to be achieved whilst also allowing the ADR to interface with a 4 K cryocooler. It should be noted that whilst the dADR has been designed to operate from 4 K (based on current space cryocooler technology), there is flexibility in the design to enable the dADR to operate from a wide range of bath temperatures.

A 3D engineering model and photograph of the dADR are shown in Fig. 2. The operational procedure for the ADR is: (1) simultaneous magnetization of both pills with both heat switches closed in order to transfer the heat of magnetization to the 4 K bath; (2) the heat switch between the bath and high temperature stage is opened and the high temperature stage is demagnetized with the heat switch between the high and low temperature stages remaining closed in order to cool the low temperature stage (demagnetization is not adiabatic); (3) the heat switch between the high and low temperature stages is opened and the low temperature stage is demagnetized to the required operational temperature (demagnetization is very close to adiabatic); (4) the low temperature stage is held at the required operational temperature (e.g. 50 mK) via computer control of the magnets while the high temperature stage warms under parasitic thermal load.

There are three main components to the ADR design; paramagnetic materials, heat switches and magnets, each of which is discussed in turn below. The driver for the design was to modularise the ADR so that each component can be replaced independently if and when better technology becomes available.

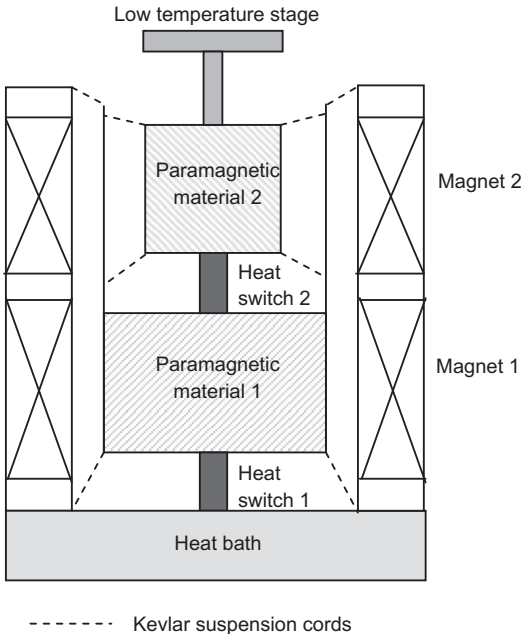


**Fig. 1.** Schematic of dADR.

### 2.1. Paramagnetic materials

The ADR was built using two paramagnetic materials; chromium potassium alum (CPA) and dysprosium gallium garnet (DGG). CPA was used as the low temperature refrigerant with an operating temperature range of 1.6 K to 25 mK. The pill is a compressed pill; 0.56 mol of ground CPA crystals were compacted around gold plated copper wires within the pill casing which connect to the cold finger. This method allowed for a high packing density of approximately 95%. A 0.9 mol single crystal of DGG was used for the high temperature stage and operates in the temperature range of 4–0.6 K [3]. It has a diameter of 57 mm and a height of 96 mm (see Fig. 3). Thermal interfacing to the crystal was achieved via mechanical compression using indium to enhance the thermal connection.

### 2.2. Heat switches

Two types of heat switch are used in the ADR; a gas-gap heat switch which was supplied by CEA, France [4] and was originally developed for the Herschel and Planck ESA missions; a superconducting lead heat switch comprising of lead wire wrapped around a low thermally conducting Vespel™ SP22 rod. The former is used between the DGG and the heat bath and the latter between the CPA and DGG. Table 1 gives the thermal properties of both switches in their 'on' (thermally conducting) and 'off' (thermally isolating) states. It should be noted that due to the configuration of the ESA ADR, the thermal conductance of the gas-gap heat switch is limited in the 'on' state by the thermal conductivity of the copper strap connecting it to the DGG and is dominated by the thermal conductivity of the titanium tube within the gas switch itself in the 'off' state (the thermal conductivities of copper and titanium are also given in Table 1).

### 2.3. Magnet system

The details of the magnet design are presented in Milward et al. [6]. In summary, the magnet system has two sections, one for each of the paramagnetic materials. Each section is comprised of five magnets; a main coil, two field compensating coils situated at the end of the main coil to boost the end field and two stray magnetic field control coils which reduce the stray magnetic field to acceptable levels for the sample volume and the spacecraft. All 10 coils have been wound using 0.1 mm diameter NbTi superconducting wire with a total length of 235 km of wire being used for the complete system. A central magnetic field flux density of 3 T (30,000 G) for each paramagnetic material is generated using $\leqslant$2.4 A.

The complete magnet system has a total length of 400 mm, an outer diameter of 215 mm and a bore diameter of 65 mm. The magnetic shielding design proposed in Hepburn et al. [1] was implemented and the design requirements for the stray magnet field to be <5 μT at the detector focal plane and <67 μT at a distance of 0.5 m away from the centre of the ADR have been met according to model predictions. The modelled magnetic flux density profile surrounding the ADR is shown in Fig. 4. The magnetic field surrounding the ADR and cryostat was measured to be in the region of 60 μT (±10 μT) which is the local Earth's magnetic field.

### 2.4. Ground test cryostat

The engineering model ADR has been installed and tested in a ground test cryostat cooled via a Cryomech PT407 pulse tube

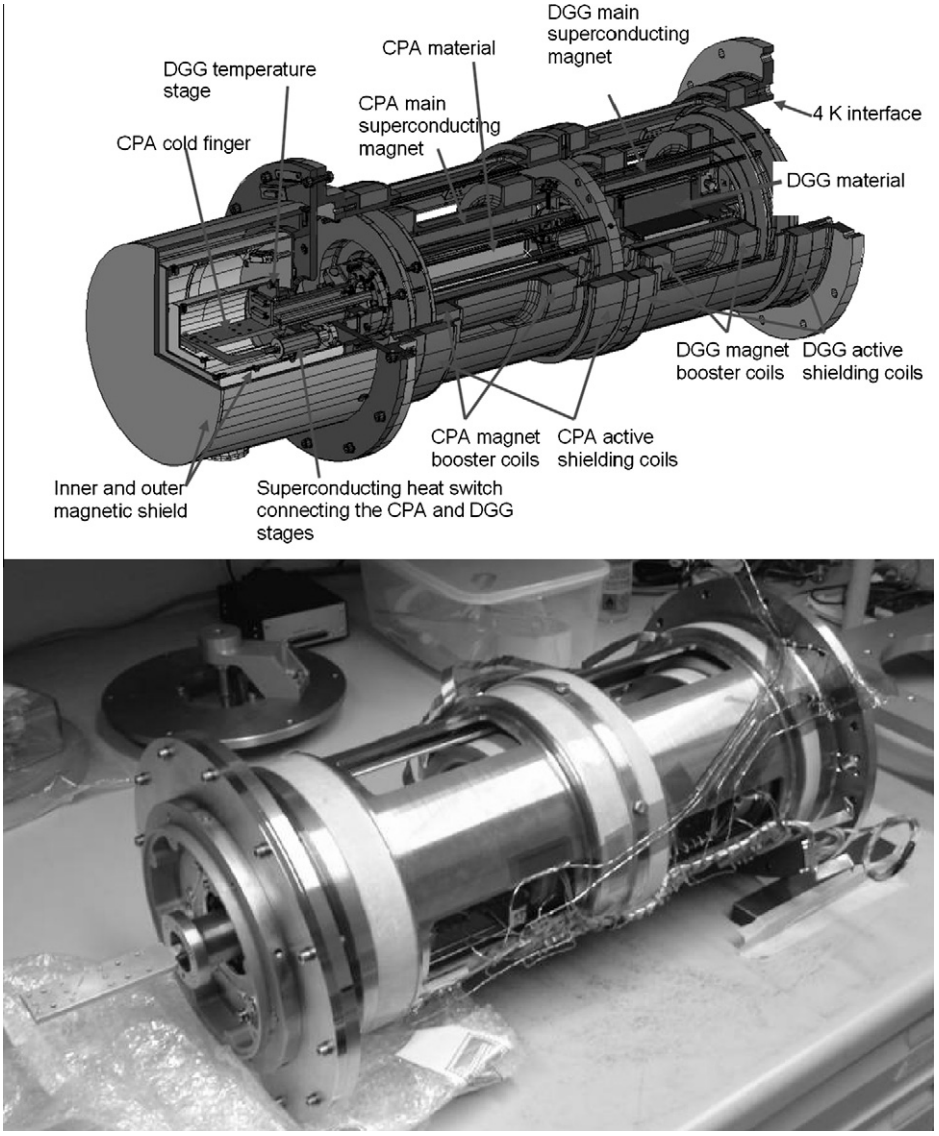


**Fig. 2.** 3D model (top) and photograph (bottom) of engineering model dADR.

**Fig. 3.** Single crystal of dysprosium gallium garnet (DGG) used in EM dADR.

(which provides a base temperature of 3.8 K) as shown in Fig. 5. The cryostat mass is not representative of a future flight system since this is a pressure vessel and therefore heavier than would be required for space. It does however include all magnetic shielding necessary for a flight model.

### 2.5. System mass

A breakdown of the mass of the ADR is given in Table 2. The total mass is approximately 45 kg including magnetic shielding and about 32 kg excluding the magnetic shielding. A significant mass reduction is anticipated by using MR heat switches and either: (1) operating the dADR from a lower bath temperature or (2) developing a continuous ADR comprising of two dADRs operating in a tandem configuration; the hold time of each dADR would only have to just exceed the recycle time, therefore allowing for a dramatic reduction in size of the pills and Kevlar suspension cords and hence resulting in a reduction in overall size and mass of the ADR. This is discussed further in Section 5 of this paper.

### 2.6. Space pre-qualification

The ADR has been vibration tested and has passed pre-qualification for an Ariane 5 launch at sub-system level. Due to the financial

**Table 1**
Thermal properties of superconducting lead and gas-gap heat switches used in the ESA ADR.

| Heat switch | 'On' state | 'Off' state |
|---|---|---|
| Superconducting lead (based on measured performance) | 0.01 K $\leqslant T \leqslant$ 2.85 K: $k = 0.52\ T^{2.97}$ W cm$^{-1}$ K$^{-1}$ | 0.01 K $\leqslant T \leqslant$ 3.00 K: $k = 0.0296\ T^{3.0569}$ W cm$^{-1}$ K$^{-1}$ |
| | 2.85 K $< T \leqslant$ 4 K: $k = 9$ W cm$^{-1}$ K$^{-1}$ | 3.00 $< T \leqslant$ 3.50 K: $k = 0.2670\ T^{1.0543}$ W cm$^{-1}$ K$^{-1}$ |
| | 4 K $< T \leqslant$ 8 K: $k = 36\ T^{-1}$ W cm$^{-1}$ K$^{-1}$ | 3.50 K $< T \leqslant$ 8.00 K: $k = 0.4567\ T^{0.6256}$ W cm$^{-1}$ K$^{-1}$ |
| Gas gap [5] | $10 \times 10^{-3}$ W K$^{-1}$ at 1 K | $2 \times 10^{-6}$ W K$^{-1}$ at 1 K |
| | $42 \times 10^{-3}$ W K$^{-1}$ at 4 K | $18 \times 10^{-6}$ W K$^{-1}$ at 4 K |
| | Limited by copper strap[a]: 1.00 $< T \leqslant$ 10.00 K: $k = 0.9858\ T + 0.2816$ W cm$^{-1}$ K$^{-1}$ | Dominated by titanium tube [5]: 0.30 K $\leqslant T \leqslant$ 2.00 K: $k = 4.32 \times 10^{-4}\ T^{1.59}$ W cm$^{-1}$ K$^{-1}$ |
| | | 2.00 K $\leqslant T \leqslant$ 13.00 K: $k = 5.88 \times 10^{-4}\ T^{1.1}$ W cm$^{-1}$ K$^{-1}$ |

[a] Based on measured performance.

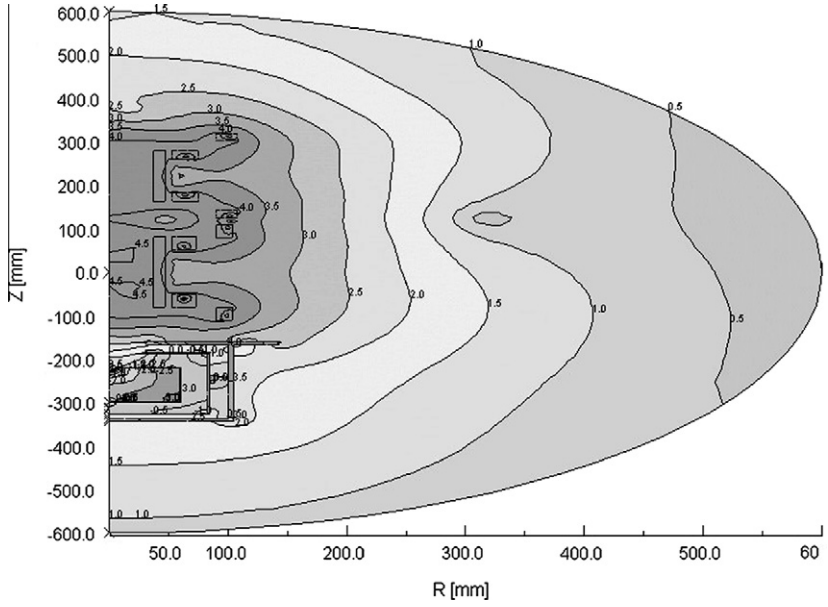


**Fig. 4.** Modelled magnetic flux density profile surrounding the ADR.

cost of the ADR it was agreed (with the ESA) that the system would not undergo vibration as a whole system but that it would be performed at sub-system level. Qualification was in three main areas; the Kevlar suspension system, magnet sub-assembly and the superconducting lead heat switch. The vibration levels at which each of these sub-systems underwent are tabulated in Table 3.

*2.6.1. Kevlar suspension system*

A mass dummy of the pills was used for the testing of the Kevlar suspension system. The pills are suspended at each end by Kevlar, tensioned by the use of Belleville springs at one end of the pill suspension system. As the pill system is axially symmetric only two directions, longitudinal and axial are possible. Three accelerometers were mounted at each end of the mass dummy, measuring the vertical, horizontal and axial accelerations. Figs. 6 and 7 show the low level sine sweep, which is used to identify resonances, in the transverse and axial (longitudinal) direction. Two control accelerometers were mounted next to the unit to monitor the vibration.

In the transverse direction six resonant modes where measured in two distinct groups (100–300 Hz and 600–800 Hz), the first mode measuring <1 g is at 125 Hz and is seen by the drive (vertical) and lateral sensors at both ends of the mass dummy. The second mode at 153 Hz has a slightly greater response at about 2 g from all components, although for the axial direction, flange and plunger the response is mild (about 0.2 g). The flange and plunger are components used to provide tension to the Kevlar suspension system.

In the longitudinal direction, the main resonance is a broad feature between 200 and 300 Hz at a level of about 2 g. There appears to be two main longitudinal modes at 225 and 245 Hz which is likely to be due to the dummy mass being suspended slightly off-centre causing cross coupling to two slightly different axial modes.

*2.6.2. Magnet sub-assembly*

The magnet sub-assembly of the ADR comprises three shells. The inner shell houses the main coil for magnetizing the CPA and DGG stages. A middle shell houses booster coils which are co-located with the ends of the main coils, in order to enhance the magnetic field locally. An outer shell contains coils in an opposing polarity in order to contain the magnetic field. In order to test the magnet system one real superconducting magnet coil on the outer magnet former was wound with all the other coils represented by mass dummies. The cryogenic operation of the superconducting coil was tested prior to vibration and then re-tested post vibration. The system passed the longitudinal axis sine and random vibration, with no obvious resonances, but during transverse axis vibration material failure occurred in the outer magnet shell. In order to allow for thermal movement between the magnet shells the middle shell is anchored in the centre to the other two

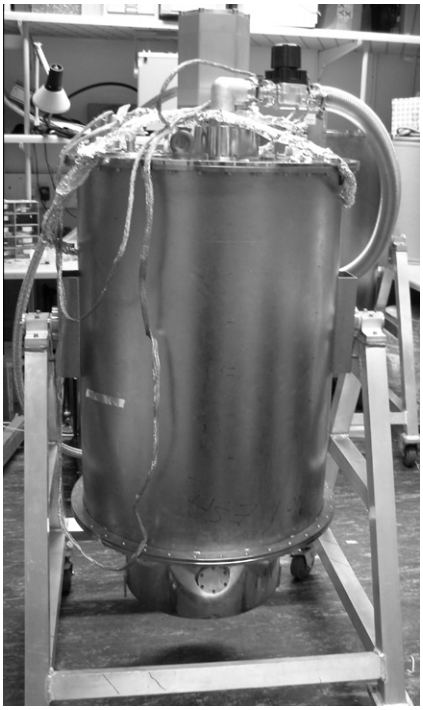

**Fig. 5.** Ground test cryostat.

**Table 2**
Mass breakdown of EM dADR.

| Sub-system | Assembly component | Mass (kg) |
|---|---|---|
| Paramagnetic including cold finger | Complete CPA and DGG assembly including cold finger | 5.526 |
| | *CPA mass* | *0.25* |
| | *DGG mass* | *0.9* |
| Magnet | Magnet assembly (of which 11.196 kg is superconducting wire) | 24.080 |
| Magnetic shielding | Focal plane magnetic shield (passive shield) | 12.9 |
| Heat switches | Gas switch | 0.127 |
| | Superconducting lead switch | 0.097 |
| Miscellaneous | Miscellaneous ADR parts | 1.942 |
| Sub total | | 44.672 |

shells, with the shell ends being a sliding fit. During vibration knocking of the middle shell into the outer shell occurred at the ends causing fracture of the material (aluminium silicon carbide). A new design which holds the magnet shells more firmly has been proved by Finite Element analysis. It is important to note that although the material had a minor failure the superconducting coil was unaffected and no change in cryogenic performance was observed when the superconducting coil was re-tested.

*2.6.3. Superconducting lead heat switch*

The superconducting switch thermal conductance was measured prior to and after vibration with no noticeable change in performance. Resonances were observed at 150, 230 and 300 Hz.

## 3. Performance of the EM ADR

At the time of delivery in July 2008, the EM ADR performed as follows: the recycle time was 15 h, the hold time at 50 mK (with an average parasitic heat load of 2.34 μW) was 10 h and the base temperature of the system was 25 mK, thus enabling the target

**Table 3**
Vibration specification.

| Test | Frequency (Hz) | Level |
|---|---|---|
| Sine vibration | 5–18 | ±11 mm |
| | 18–60 | ±15 g |
| | 60–100 | ±7.5 |
| | Sweep Rate | 2 oct./min* |
| Random vibration | 20–100 | +3 dB/oct. |
| | 100–300 | 0.1 $g^2$/Hz |
| | 300–2000 | −9 dB/oct. |
| | Composite | 6.3 g (rms) |
| | Duration | 2.0 min/axis |

temperature of 30 mK to be achieved. (Note, an average parasitic heat load is given since the DGG temperature increases during the hold time and therefore the subsequent parasitic heat load is not constant.) In comparison the design requirements were a recycle time of 4 h and a hold time at 50 mK of 24 h with a 1 μW applied heat load (in addition to parasitic load). A hold time of 2.2 h at 30 mK with only parasitic load was measured. During the 10 h hold time at 50 mK the thermal stability was measured to be ±8 μK.

The EM ADR has been fully modelled using a mathematical thermal model which can calculate the heat loads via the ADR components (heat switches, Kevlar, radiation, wiring) and the resulting effect on the temperatures of the DGG and CPA. This model has been proven to be in excellent agreement with the experimental results (Bartlett [7]) and has therefore been a useful tool in analysing the performance of the ADR and its limitations.

There are two limitations in the performance of the ADR which are discussed below: the base temperature of the ADR which is limited by thermal boundary resistance (TBR); the superconducting lead heat switch which, due to its low 'on' thermal conductivity and high 'off' thermal conductivity results in a long ADR recycle time and a short hold time. It is also shown that operating the dADR from a lower bath temperature would improve performance.

### 3.1. Base temperature of the ADR and thermal boundary resistance

At low temperatures, in non-electrically conducting materials, heat is transferred by the conduction of phonons. Problems arise when materials are brought into thermal contact with one another as the exchange of phonons between the materials at very low temperatures (sub 150 mK) is not sufficient to keep the materials in thermal equilibrium, resulting in a thermal boundary.

The heat transfer across the boundary has been derived by Ambler and Hudson [8] to be:

$$\frac{dQ}{dt} = \frac{\beta A}{3}(T_1^3 - T_2^3) \tag{1}$$

where $dQ/dt$ is the heat flow across the boundary, $A$ is the contact area, $T_1 - T_2$ the temperature difference across the boundary and $\beta$ the thermal transport parameter.

The value of the thermal transport parameter $\beta$ was determined by Mendoza [9] to be $3 \times 10^{-5}\,\mathrm{W\,cm^{-2}\,K^{-3}}$, whereas Goodman [10] obtained a higher value of $6.7 \times 10^{-4}\,\mathrm{W\,cm^{-2}\,K^{-3}}$. Based on the analysis of the performance of the EM ADR and using the mathematical thermal model created to simulate the ADR performance, a value of $\beta$ of $4 \times 10^{-4}\,\mathrm{W\,cm^{-2}\,K^{-3}}$ has been derived from our measurements.

The CPA pill used in the EM ADR is a compressed pill as previously mentioned. The gold plated copper wires within the pill casing are connected to a long (20 cm) cold finger. The temperature of the CPA pill (e.g. 25 mK) is measured at the far end of this cold finger. The thermal boundary arises between the copper and CPA interface, therefore although the CPA crystals themselves reach a

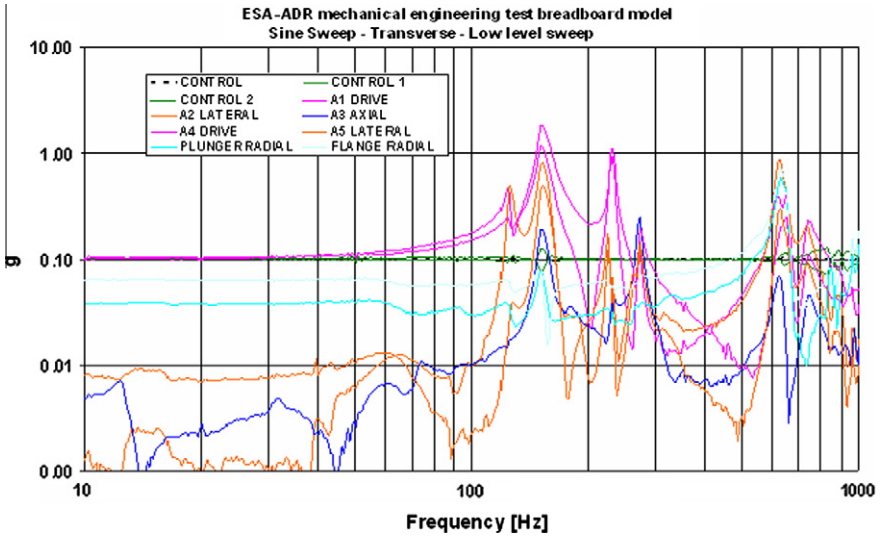


**Fig. 6.** Low level sine sweep (transverse) vibration response.

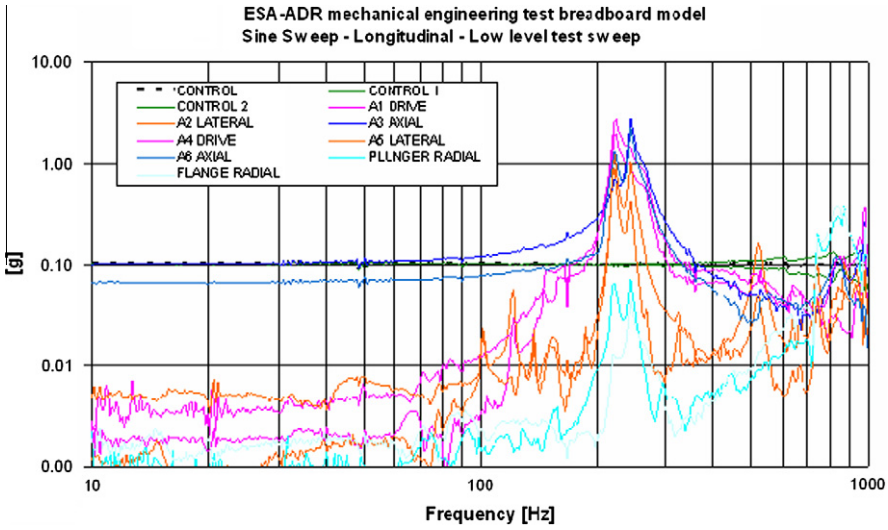


**Fig. 7.** Low level sine sweep (longitudinal) vibration response.

temperature close to the Néel temperature of 10 mK (based on modelling), the cold finger only reaches a temperature of 25 mK. In order to ensure that this temperature difference was only due to the thermal boundary resistance and not an additional heat load to the thermometer via wiring, two different ruthenium oxide thermometers were used simultaneously (of different sizes and contact areas) and both were in agreement to within a few mK. It should be noted that due to the dADR design, it is the cold finger that is directly connected to the DGG stage via the lead heat switch and therefore any heat load to the CPA (with the exception of the heat load via the Kevlar cords) must travel via the cold finger which is not the ideal thermal path.

Eq. (1) shows that there are two factors which can reduce the achievable temperature on the cold finger: (1) the heat load to the cold finger (and hence the CPA pill) from the DGG (i.e. parasitic load) and (2) the contact area between the two materials in the pill. Fig. 8 shows how the minimum cold finger temperature is predicted to vary with the heat load across the boundary within the pill, with the heat load varied between 5 nW and 2 μW. Only with an incredibly low heat load of 5 nW can the predicted minimum cold finger temperature be reduced to 10 mK; the current measured parasitic heat load to the CPA pill via the cold finger (i.e. excluding the Kevlar) is 0.6 μW and therefore a temperature below 25 mK cannot be reached.

The contact area of the copper wires with the CPA crystals in the EM ADR is 300 $cm^2$. Fig. 9 shows how the minimum cold finger temperature is predicted to vary with contact area for a 0.6 μW heat load (based on the current system configuration). The figure shows that 10 mK cannot be achieved for a heat load of 0.6 μW even with a contact area of 5000 $cm^2$ (which would be a huge increase in the volume of wire and hence the pill). Increasing the area to 1000 $cm^2$ would enable 18 mK to be reached which would be an improvement with the potential to operate the ADR at 20 mK. Increasing the contact area further would only result in a marginal decrease in cold finger temperature.

In conclusion, thermal boundary resistance is the limiting factor of the achievable cold finger temperature and obtaining a base temperature below 25 mK when heat loads of the order of microwatts are present is a very difficult task.

### 3.2. Superconducting lead heat switch

The total parasitic heat load to the CPA (including the heat load via the Kevlar) from the DGG at the beginning of the hold time is

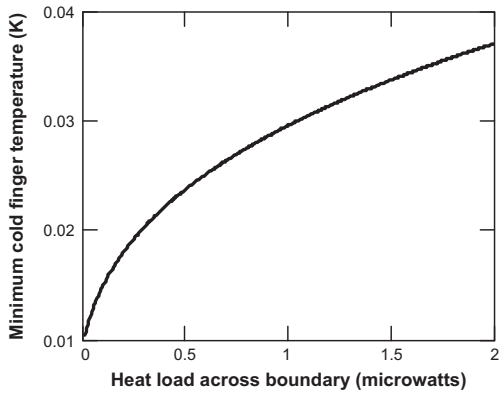


**Fig. 8.** Predicted dependence of minimum cold finger temperature with heat load across the boundary.

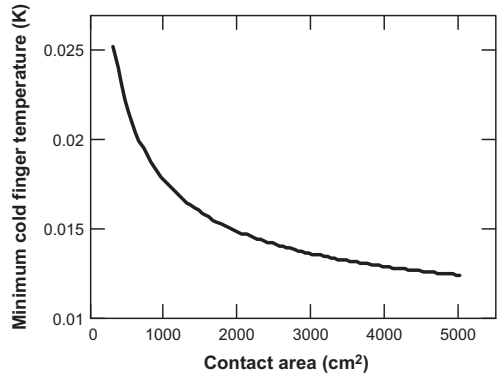


**Fig. 9.** Predicted dependence of cold finger temperature with contact area.

1.02 μW (DGG temperature is about 0.9 K). The dominant contribution to this heat load is via the superconducting lead heat switch which contributes 0.57 μW. The DGG temperature increases throughout the hold time thereby increasing the parasitic heat load to the CPA pill; at the end of the hold time the DGG temperature is about 1.3 K which gives a total parasitic heat load onto the CPA of 3.26 μW, of which 2.30 μW is via the lead heat switch. Such a large heat load has a significant effect on the hold time of the ADR. Fig. 10 shows how the total parasitic heat load to the CPA from the DGG (with the CPA at 50 mK) varies with DGG temperature and also shows the contributions to the total heat load from the heat switch, Kevlar and radiation and wiring.

Another consequence of the lead heat switch is its poor normal 'on' state thermal conductivity (see Table 1, Section 2.2) which increases the recycle time due to its inefficiency of extracting the heat of magnetization and pre-cooling of the CPA (prior to the CPA demagnetization). Replacing the superconducting lead switch which is a relatively easy task due to the modular design of the ADR, with a better heat switch with a higher switching ratio will enable the ADR to have a longer hold time and a shorter recycle time (as well as the potential for a lower base temperature). An ideal candidate is a single crystal tungsten magnetoresistive (MR) heat switch which is under development at MSSL (see Section 4).

### 3.3. Operating the EM dADR from a lower bath temperature

The EM ADR has been designed to operate from a 4 K bath provided by a space cryocooler, namely the 4 K Joule–Thomson cooler flown on the ESA mission Planck. However, the dADR has the flexibility of being able to operate from a wide range of bath temperatures. New space cryocooler technology could mean that the dADR is operated from a bath temperature of 2.5 K or even 1.8 K (as is anticipated for IXO). Based on this and using the mathematical thermal dADR model to simulate the performance, it is expected that the delivered EM ADR (i.e. with no modifications) will have the following performance if operated from lower bath temperatures: recycle time of 15 h and a hold time of 22 h (0 μW applied and a time averaged parasitic load of 1.26 μW) and 13 h (1 μW applied and a time averaged parasitic load of 1 μW) for a 2.5 K bath; recycle time of 15 h and a hold time of 34 h (0 μW applied and a time averaged parasitic load of 0.85 μW) and 17 h (1 μW applied and a time averaged parasitic load of 0.7 μW) for a 1.8 K bath temperature. However, significant improvement is anticipated when the lead heat switch is replaced with the MR heat switch.

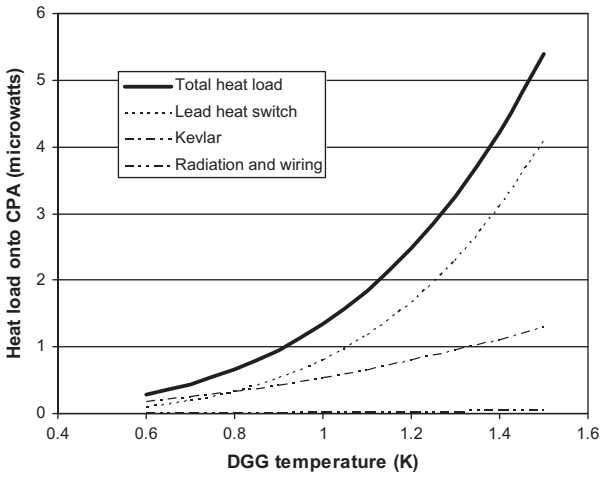


**Fig. 10.** Modelled parasitic heat loads onto 50 mK CPA as a function of DGG temperature (lead heat switch).

## 4. Component replacement for improved performance of the EM ADR

The performance of the EM ADR is to be improved in the first instance by replacing the superconducting lead heat switch with a tungsten MR heat switch and in the second instance by also replacing the gas-gap heat switch with a MR heat switch. Replacing the former will greatly increase the hold time and reduce the recycle time whilst replacing the latter will further decrease the recycle time (this is important for a continuous system as discussed later).

In metals, heat is conducted by electrons and phonons with the former being the dominant process. In magnetoresistive materials, which are compensated metals with closed Fermi surfaces, electronic conduction can be suppressed by the application of a magnetic field in a direction perpendicular to that of the electron flow, with the heat conducted due to electrons decreasing with increasing magnetic field. This can ultimately result in the thermal conductivity being dominated by phonons. Switching is therefore achieved by the application and removal of an external magnetic field; the 'on' highly thermally conducting state refers to the dominant conduction by electrons (no magnetic field) and the 'off' low thermally conducting state refers to the dominant conduction by phonons (magnetic field is applied). An advantage of the MR switch is that switching is therefore instantaneous in comparison to the gas-gap heat switch used in the EM ADR.

A picture of the current MR switch, which is based on a design by Canavan et al. [11] and has been tested at MSSL, is shown on the

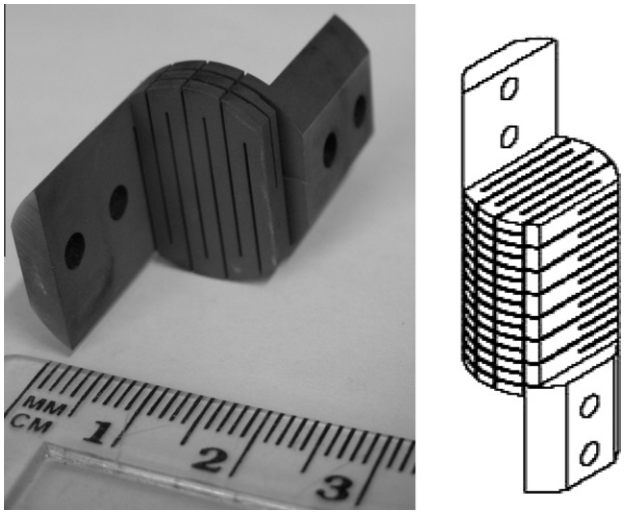


**Fig. 11.** Tungsten MR heat switch under development at MSSL: three layer switch (left); drawing of 15 layer switch (right).

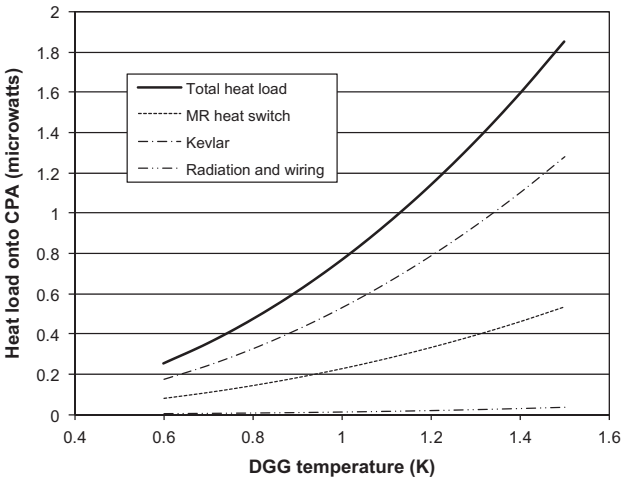


**Fig. 12.** Modelled parasitic heat loads onto 50 mK CPA as a function of DGG temperature (MR heat switch, 5× length).

**Table 4**
Thermal conductivities of the MR switch at set temperatures (based on an interpolation of measured results).

| Temperature (K) | 'On' thermal conductivity ($W\,cm^{-1}\,K^{-1}$) | 'Off' thermal conductivity ($W\,cm^{-1}\,K^{-1}$) |
|---|---|---|
| 0.05 | 2.80 | $2.10 \times 10^{-4}$ |
| 0.5 | 40.32 | $2.14 \times 10^{-3}$ |
| 1 | 90.01 | $4.50 \times 10^{-3}$ |
| 2 | 200.97 | $1.08 \times 10^{-2}$ |
| 3 | 321.51 | $2.07 \times 10^{-2}$ |
| 4 | 448.72 | $3.60 \times 10^{-2}$ |

left in Fig. 11. It has three layers, a free path length of 43 cm and a 1.5 × 1.5 mm cross section. The switch has a height of 5.1 mm (excluding the mounting flanges) and a diameter of 2 cm. Table 4 gives a summary of the 'on' and 'off' thermal conductivities of the MR switch at specific temperatures which have been interpolated from the measured thermal conductivity data given in Bartlett et al. [12]. Mathematical thermal modelling based on the measured thermal conductivity has shown that this switch will have a significant effect on the performance of the EM ADR but to achieve the required 24 h hold time at 50 mK with a 1 μW heat load, a five times longer switch will be required, a drawing of which is shown on the right in Fig. 11.

Using this switch instead of the superconducting lead heat switch, the predicted performance of the EM ADR is: a recycle time of 6 h; a hold time at 50 mK of 24 h with an applied heat load of 1 μW (and an average parasitic heat load of 0.95 μW) and a cold finger base temperature of 18 mK (due to the reduced heat load on the cold finger). Such an improvement in hold time is due to: (1) the lower CPA temperature achieved prior to its demagnetization (the MR switch provides a better thermal link between the DGG and CPA during DGG demagnetization therefore allowing the CPA to reach a lower temperature) and (2) the lower parasitic heat load onto the CPA from the DGG via the MR heat switch (compared to the superconducting lead heat switch). Fig. 12 shows how the total parasitic heat load to the CPA from the DGG (with the CPA at 50 mK) varies with DGG temperature and also shows the contributions from the MR heat switch, Kevlar and radiation and wiring. Note, comparing Figs. 10 and 12 allow for a direct comparison between the performances of the superconducting lead and MR heat switches under the same conditions.

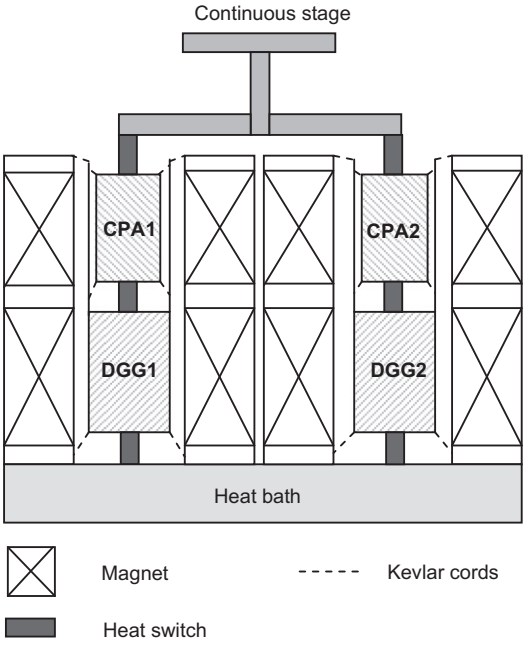


**Fig. 13.** Schematic of a continuous tandem ADR.

Replacing the gas-gap heat switch with a MR switch is predicted to further improve performance giving a predicted recycle time of under 2 h and a hold time of 29 h with an applied 1 μW heat load (and an average parasitic heat load of 0.63 μW). This would enable the EM dADR to fulfil all the design requirements of the ESA contract.

The performance could be further improved by operating the dADR from a lower bath temperature. Operating from a base temperature of 2.5 K would give a recycle and hold time (at 50 mK with a 1 μW applied heat load) of 6 and 41 h (with average parasitic heat load of 0.2 μW) by just replacing the lead heat switch with the MR heat switch whilst 2 and 45 h (with an average parasitic heat load of 0.15 μW) is anticipated by replacing both the lead and gas-gap heat switches. This improved performance would allow the EM ADR to exceed the required hold time of 24 h allowing for a reduction in mass of the dADR; sizing for a 24 h hold time and based on the dADR using 2 MR heat switches, the paramagnetic

**Table 5**
Estimated mass breakdown of CADR.

| Component | Mass (kg) |
|---|---|
| Paramagnetic materials | 0.1 |
| Magnet | 2.4 |
| Magnet former | 1.0 |
| Pill supports and structure | 0.5 |
| Contingency | 0.5 |
| | 4.5 |

materials and Kevlar diameter could be reduced by a factor of 2. In addition, with optimisation of the magnet, we anticipate an ADR mass of 10 kg (excluding focal plane magnetic shielding). Since the dominant heat load to the CPA during the hold time is from the applied heat load and not the parasitic load from the DGG, there is little to gain in operating the ADR from a lower bath temperature.

## 5. Extension to continuous operation

Continuous operation can be achieved by operating two dADRs in a tandem configuration. Both are connected to a continuous stage via heat switches with one dADR maintaining the operational cold finger temperature whilst the other is recycling. A schematic of a continuous ADR (CADR) is shown in Fig. 13. Continuous cooling and tandem operation have implications on the performance and the design of each dADR: (1) the hold time must exceed the recycle time but only by a small margin and therefore the size of each dADR can be reduced; (2) operating two dADRs in tandem imposes an additional heat load onto the cold finger due to the connection via a heat switch to the recycling dADR. This has an affect on the hold time as well as the thermal stability of the continuous stage.

The CADR has been designed using the mathematical thermal model which has been proven to correctly simulate the operation of the EM ADR (as mentioned above). The basis of the dADR unit within the CADR system is the EM ADR using MR heat switches which therefore gives us confidence in the CADR design. The full extent of the modelling behind the CADR design is presented in Bartlett [7] with a summary of the design outlined below.

Size reduction is dependent on several factors: (1) the ability to extract heat from the paramagnetic materials quickly and efficiently; (2) the maximum allowable magnet ramp rate; (3) the maximum allowed heat load to the 4 K stage via a heat switch (5 mW); (4) the switching ratio(s) of the heat switch(es) used and (5) the maximum recycling temperature of the CPA. Each of these has a considerable effect on the recycling and hold times of a dADR and hence the size reduction.

The design of the CADR and hence the size reduction of the dADR unit within the CADR has been limited by: the hold to recycle time ratio which we have set to be 1.5:1 to allow some margin for error; the heat load to the cold finger via a heat switch from the recycling ADR which we have set to a maximum of 1 μW so as not to be a dominant load.

The size of the CADR has been investigated using the mathematical thermal model for the EM ADR using the MR heat switch and a reduction in magnet ramp rate from our current 25 min to 10 min, which is anticipated for a revised magnet. For a 4 K bath, our investigation concludes that the size of the paramagnetic materials and the cross sectional area of the Kevlar can be reduced by a factor of 24. Reducing the bath temperature to 2.5 K and 1.8 K allows for a reduction in size of the EM ADR of a factor of 35 and 40 respectively.

This clearly offers a considerable mass saving. Based on operation from a 4 K bath, we have a system design and estimate the ADR mass to be 4.5 kg which is broken down in Table 5. The current CADR design has a 400 mm diameter and a 600 mm length.

## 6. Conclusion

An engineering model dADR has been developed and tested which has passed vibrational qualification for an Ariane 5 launch at sub-system level. The dADR has a base temperature of 25 mK, a measured hold time at 50 mK of 10 h and a recycle time of 15 h. The main performance limitation has been identified to be the superconducting lead heat switch. By replacing this with a magnetoresistive heat switch, the hold time is anticipated to increase to 24 h with a 1 μW applied heat load (based on thermal measurements of the magnetoresistive switch) which meets the requirements of the ESA contract. By also replacing the gas-gap heat switch, the recycle time could be reduced to about 2 h resulting in the EM ADR fulfilling all requirements.

The dADR design to obtain 50 mK offers flexibility as it can be operated from wide range of bath temperatures provided by either a mechanical cooler or liquid cryogens, and versatility due to its modularisation. Replacing both the heat switches and operating from a lower bath temperature of 2.5 K allows for a reduction in mass.

Operating two dADRs in a tandem configuration will provide continuous operation allowing for a dramatic reduction in mass. This is possible due to a reduction in size of the paramagnetic materials and diameter of the Kevlar suspension cords. It has been calculated that these can be reduced in size by a factor of 24 (for a 4 K bath), factor of 35 (for 2.5 K bath) and a factor of 40 (for a 1.8 K bath). For the 4 K bath, this would result in a continuous system with a mass of ~4.5 kg.

The detailed modelling and understanding of the performance of the EM ADR mean that a smaller, lighter system can be evolved from the EM ADR which can fulfil the requirements of future space missions such as IXO.

## Acknowledgements

This work has been supported by the European Space Agency and the Science and Technology Facilities Council, UK (STFC).

## References

[1] Hepburn ID, Brockley-Blatt C, Coker P, Crofts E, Winter B, Milward S, et al. Space engineering model cryogen free ADR for future ESA space missions. Adv Cryog Eng 2004;49:1737–45.
[2] Hepburn ID, Brockley-Blatt C, Coker P, Crofts E, Winter B, Hardy G, et al. Design and development of a space engineering model cryogen free ADR for future ESA space missions. In: CryoPrague 2006, proceedings of ICEC 21, twenty first international cryogenic engineering conference, Icaris Ltd.; 2006. p. 323–6.
[3] DGG crystal grown by The Crystal Consortium (TCC) Ltd., Glasgow (UK). (It should be noted that TCC are no longer trading.)
[4] Duband L. A thermal switch for use at liquid helium temperature in space-bourne cryogenic systems. In: Proceedings of the 8th international cryocooler conference. Vail (CO, USA): Plenum Press; 1995. p. 731–41.
[5] L. Duband, private communication.
[6] Milward S, Harrison S, Stafford-Allen R, Hepburn I, Brockley-Blatt C. Design, manufacture and test of an adiabatic demagnetization refrigerator magnet for use in space. IEEE Trans Appl Supercond 2005;15(2):1477–9.
[7] Bartlett J. PhD thesis. Design of a 50 mK continuous adiabatic demagnetization refrigerator for future space missions. UCL, University of London; October 2008.
[8] Ambler E, Hudson RP. Magnetic cooling. Cryogenic Physics Laboratory, National Bureau of Standards, Washington 25, DC. Reports on progress in physics, vol. 18; 1955. p. 251–303.
[9] Mendoza E. Les Phénomènes Cryomagnétiques. Langevin-Perrin Colloquim, Collège de France; 1948. p. 53.
[10] Goodman BB. The thermal conductivity of superconducting tin below 1 K. In: Proceedings of the physical society, vol. 66A(3); 1 March, 1953. p. 217–27.
[11] Canavan ER, Dipirro MJ, Panel J, Shirron PJ, Tuttle JG. A magnetoresistive heat switch for the continuous ADR. Adv Cryog Eng 2002;47:1183–90.
[12] Bartlett J, Hardy G, Hepburn ID, Ray R, Weatherstone S. Thermal characterization of a tungsten magnetoresistive heat switch. Cryogenics 2010;50:647–52.